Supplementary information

Realization of near-perfect absorption in the whole reststrahlen band of SiC

Dongxue Chen[#], Jianjie Dong[#], Jianji Yang, Yilei Hua, Guixin Li, Chuanfei guo, Changqing Xie, Ming Liu, Qian Liu[*]

#These authors contributed equally to this work.

1. Skin depth of SiC

Skin depth S of a material is a measure of how deep any electromagnetic radiation can penetrate into a material. It can be expressed as $S = \frac{1}{2\,\mathrm{Im}(\sqrt{\varepsilon})}\frac{\lambda_0}{2\pi}$.

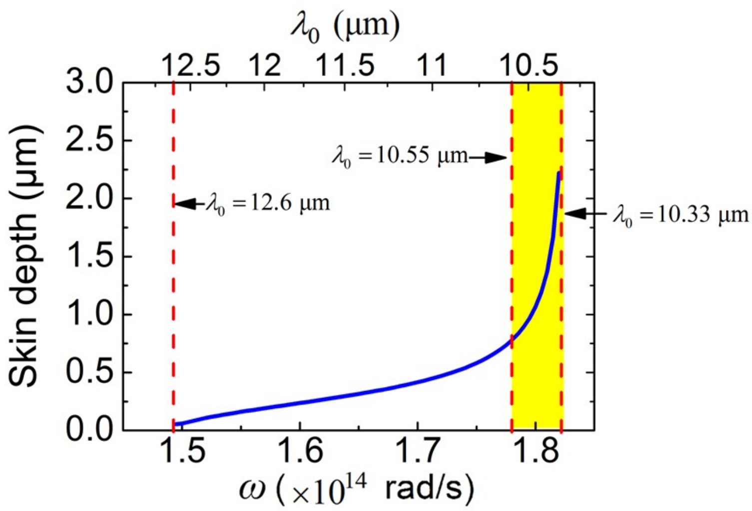

Figure S1. Skin depth of SiC in the RB. Compared with the free-space wavelength λ_0, the skin depth is very small in the range from $\lambda_0 = 10.55$ μm to $\lambda_0 = 12.6$ μm. In the range from $\lambda_0 = 10.33$ μm to $\lambda_0 = 10.55$ μm, the skin depth has a relatively large value.

2. Optimization of geometrical parameters of the CPDSS

The first factor for optimizing the geometrical parameters of the CPDSS that must be considered is the possibility of the fabrication of the CPDSS by our following fabrication methods. Because the control of the parameters of the cones is relatively difficult in experiment compared with the control of the parameters of the pillars, we first optimize the parameters of the cones. Because the cones whose L is located in the range from 2 μm to 7 μm, W is located in the range from 0.2 μm to 0.9 μm and density is about 3.18/μm^2 (i.e., there are 258 cones in the area 8μm×8μm) can be fabricated by our fabrication methods, L is limited in (2μm , 7μm) , W is limited in (0.2μm , 0.9μm) and the cone density is set to be about 3.18/μm^2. We find that a surface with only cones whose L is mainly located in the range from 4 μm to 5.7 μm (see **Figure 2b**), W is mainly located in the range from 0.4 μm to 0.7 μm (see **Figure 2b**) and density is about 3.18/μm^2 can have a large absorptivity (the red curve in **Figure S2a**). When we add some small cones between gaps of cones of this surface, the absorptivity cannot be further increased (see the blue curve in **Figure S2a**). When we uniformly reduce some cones from this surface, the absorptivity becomes small (see the green curve and the pink curve in **Figure S2a**). Therefore, L is set to be mainly located in the range from 4 μm to 5.7 μm (see **Figure 2b**), W is set to be mainly located in the range from 0.4 μm to 0.7 μm (see **Figure 2b**), and the cone density is set to 3.18/μm^2.

It can be found that the absorptivity of SiC at two edges of its RB has a drop by using the surface with only cones (**Figure S2a**). Therefore, the geometrical parameters of pillars need to be optimized for improving the absorptivity of SiC at two edges of the RB. It can be found in **Figure S2b** that when H is equal to $8.3\ \mu\text{m}$, the absorptivity has a large value at both the left edge and the right edge of the RB. It can be found in **Figure S2c** that when D is equal to $6\ \mu\text{m}$, the absorptivity has a large value at both the left edge and the right edge of the RB. It can be found in **Figure S2d** that when G is equal to $2\ \mu\text{m}$, the absorptivity has a large value at both the left edge and the right edge of the RB. In addition, the pillar array with $H = 8.3\ \mu\text{m}$, $D = 6\ \mu\text{m}$ and $G = 2\ \mu\text{m}$ can be easily fabricated by our fabrication methods. Therefore, the pillar height is set to $8.3\ \mu\text{m}$, the pillar diameter is set to $6\ \mu\text{m}$, and the pillar period is set to $8\ \mu\text{m}$.

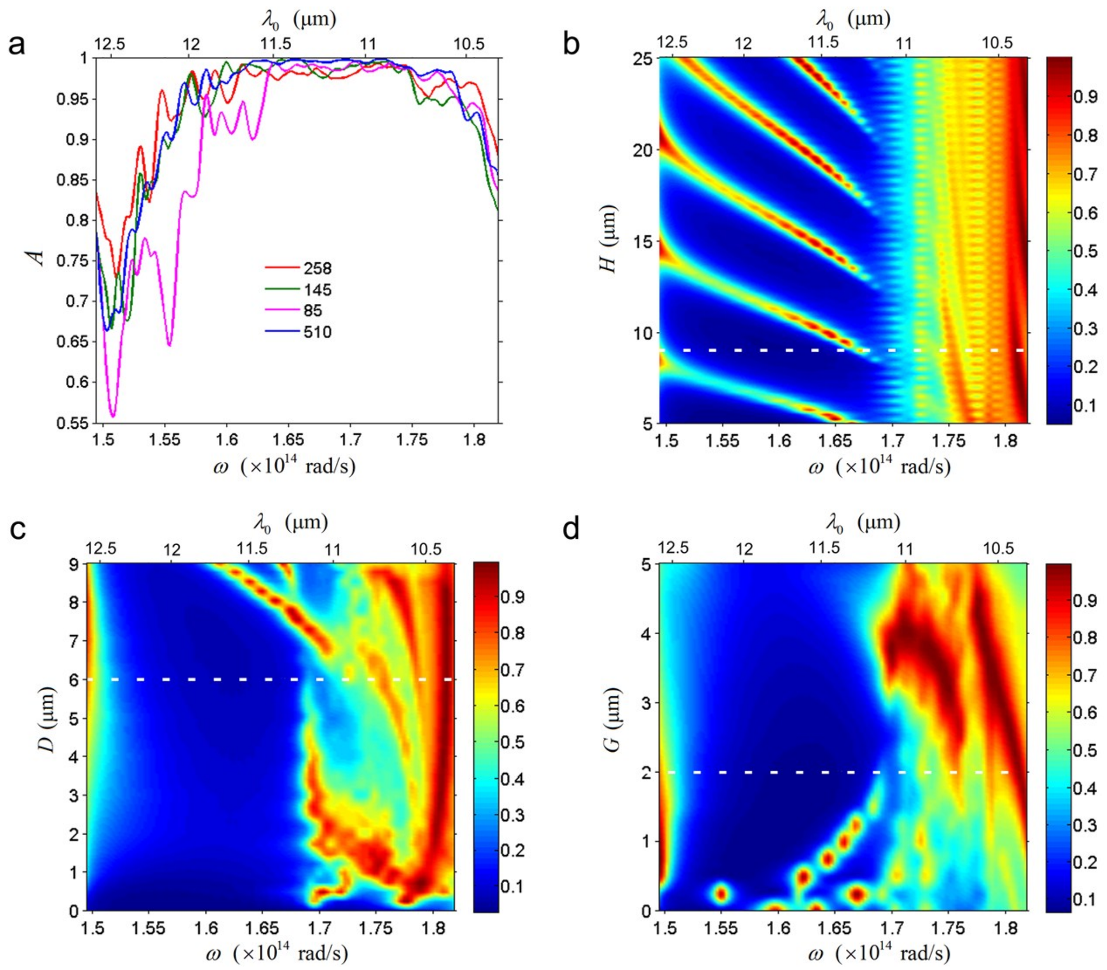

Figure S2. Optimization of geometrical parameters. a) The dependence of the absorptivity A on the number of cones in a unit cell in the RB. b) The dependence of the absorptivity on the pillar height H in the RB. $D = 6$ μm and $G = 2$ μm. c) The dependence of the absorptivity on the pillar diameter D in the RB. $H = 8.3$ μm and $G = 2$ μm. d) The dependence of the absorptivity on the pillar gap G in the RB. $H = 8.3$ μm and $D = 6$ μm.

3. Simulation results of electric field intensity distributions of the CPDSS

The finite-difference time-domain (FDTD) method was employed to simulate the interaction between electromagnetic waves and the CPDSS. The size of the simulation domain was set to 8 μm in both the x and y directions. Periodic boundary conditions were applied in both the x and y directions, and perfectly matched layers were applied in the z direction. In the x, y and z directions, the maximum mesh step was set to be smaller than $\lambda_{LO} / 200$. The incident electromagnetic wave is a plane wave. ε can be expressed as[17]

$$\varepsilon = \varepsilon_\infty (1+\frac{\omega_{LO}^2-\omega_{TO}^2}{\omega_{TO}^2-\omega^2-i\Gamma\omega}) \ ,$$

where $\varepsilon_\infty = 6.7$, $\omega_{LO} = 969\delta$ (rad/s) , $\omega_{TO} = 793\delta$ (rad/s) , $\Gamma = 4.76\delta$ (rad/s) and $\delta = 5.996\pi \times 10^{10}$

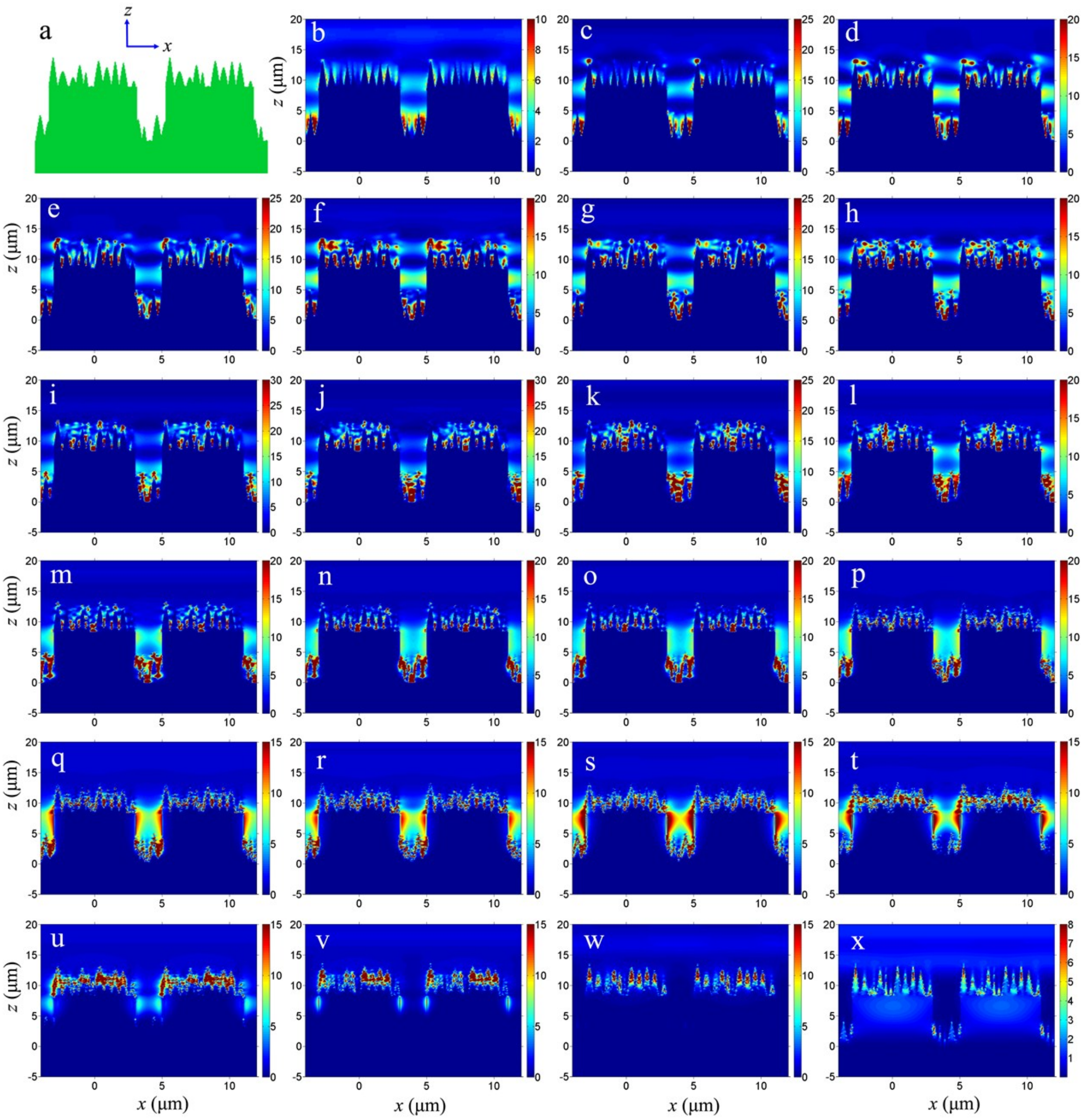

Figure S3. Normalized electric field intensity distributions. a) Cross section of the CPDSS. b) $\lambda_0 = 12.6\mu m$ ($\omega = 1.495\times10^{14}$ rad/s). c) $\lambda_0 = 12.5\mu m$ ($\omega = 1.507\times10^{14}$ rad/s). d) $\lambda_0 = 12.4\mu m$ ($\omega = 1.519\times10^{14}$ rad/s). e) $\lambda_0 = 12.3\mu m$ ($\omega = 1.531\times10^{14}$ rad/s). f) $\lambda_0 = 12.2\mu m$ ($\omega = 1.544\times10^{14}$ rad/s). g) $\lambda_0 = 12.1\mu m$ ($\omega = 1.557\times10^{14}$ rad/s). h) $\lambda_0 = 12\mu m$ ($\omega = 1.570\times10^{14}$ rad/s). i) $\lambda_0 = 11.9\mu m$ ($\omega = 1.583\times10^{14}$ rad/s). j) $\lambda_0 = 11.8\mu m$ ($\omega = 1.596\times10^{14}$ rad/s). k) $\lambda_0 = 11.7\mu m$ ($\omega = 1.610\times10^{14}$ rad/s). l) $\lambda_0 = 11.6\mu m$ ($\omega = 1.624\times10^{14}$ rad/s). m) $\lambda_0 = 11.5\mu m$ ($\omega = 1.638\times10^{14}$ rad/s). n) $\lambda_0 = 11.4\mu m$ ($\omega = 1.652\times10^{14}$ rad/s). o) $\lambda_0 = 11.3\mu m$ ($\omega = 1.667\times10^{14}$ rad/s). p) $\lambda_0 = 11.2\mu m$ ($\omega = 1.682\times10^{14}$ rad/s). q) $\lambda_0 = 11.1\mu m$ ($\omega = 1.697\times10^{14}$ rad/s). r) $\lambda_0 = 11\mu m$ ($\omega = 1.712\times10^{14}$ rad/s). s) $\lambda_0 = 10.9\mu m$ ($\omega = 1.728\times10^{14}$ rad/s). t) $\lambda_0 = 10.8\mu m$ (

$\omega = 1.744\times10^{14}$ rad/s). u) $\lambda_0 = 10.7$μm ($\omega = 1.760\times10^{14}$ rad/s). v) $\lambda_0 = 10.6$μm ($\omega = 1.777\times10^{14}$ rad/s). w) $\lambda_0 = 10.5$μm ($\omega = 1.794\times10^{14}$ rad/s). x) $\lambda_0 = 10.4$μm ($\omega = 1.811\times10^{14}$ rad/s).

4. Simulation results of Poynting vector distributions of the CPDSS

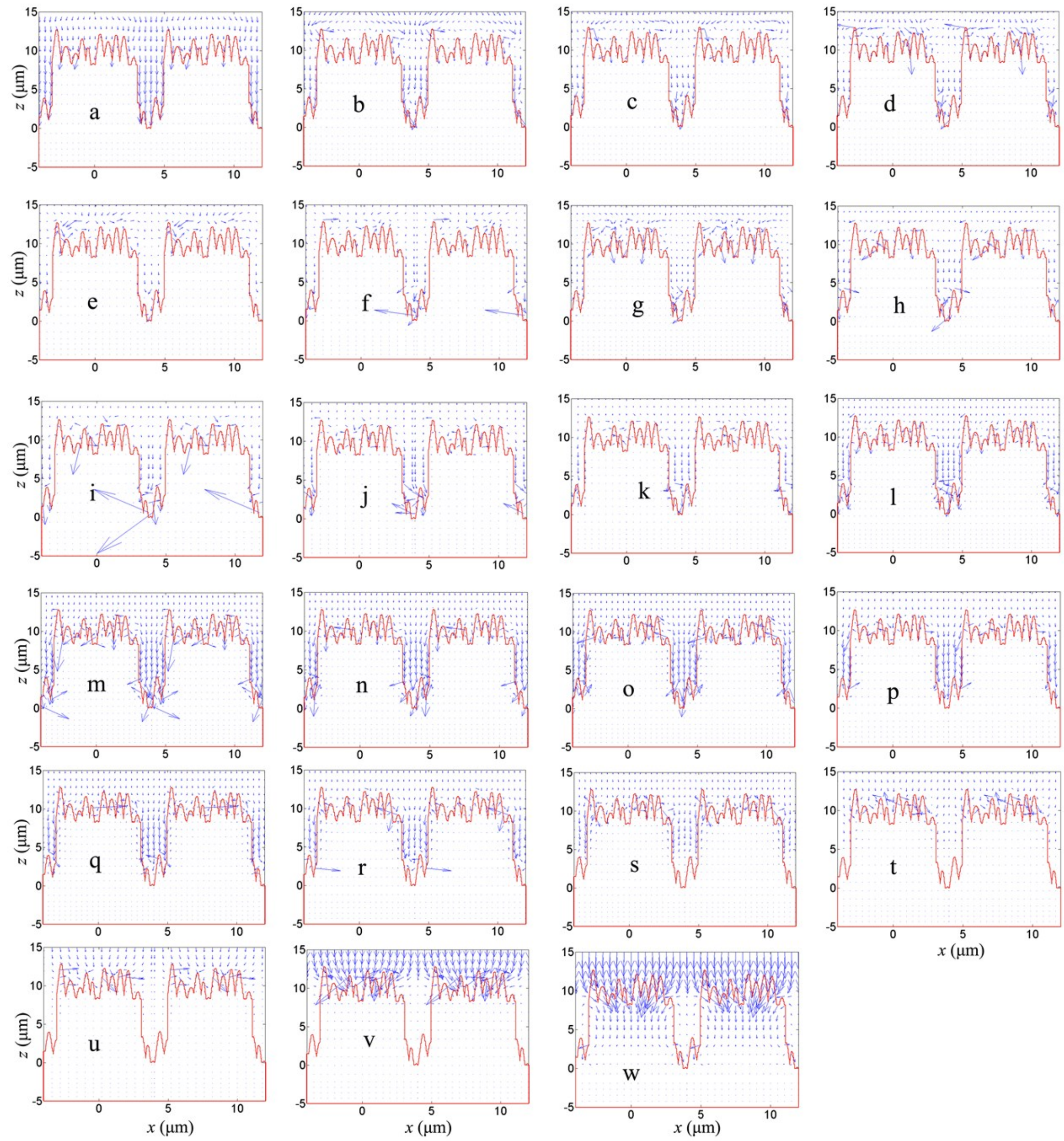

Figure S4. Poynting vector distributions. a) $\lambda_0 = 12.6$μm . b) $\lambda_0 = 12.5$μm . c) $\lambda_0 = 12.4$μm . d) $\lambda_0 = 12.3$μm . e) $\lambda_0 = 12.2$μm . f) $\lambda_0 = 12.1$μm . f) $\lambda_0 = 12$μm h) $\lambda_0 = 11.9$μm i) $\lambda_0 = 11.8$μm . j) $\lambda_0 = 11.7$μm . k) $\lambda_0 = 11.6$μm . l) $\lambda_0 = 11.5$μm . m) $\lambda_0 = 11.4$μm n) $\lambda_0 = 11.3$μm . o) $\lambda_0 = 11.2$μm . p) $\lambda_0 = 11.1$μm . q) $\lambda_0 = 11$μm . r) $\lambda_0 = 10.9$μm . s) $\lambda_0 = 10.8$μm . t) $\lambda_0 = 10.7$μm . u) $\lambda_0 = 10.6$μm . v) $\lambda_0 = 10.5$μm . w) $\lambda_0 = 10.4$μm .

5. Experimental method and characterization

Sample fabrication: A 6H-SiC (0001) wafer with polished surfaces was chosen. The fabrication steps of the CPDSS are as follows (**Figure S5**): (1) The SiC wafer was cleaned by an ultrasonic cleaner in acetone, isopropyl alcohol and deionized water for 10 min in turn; (2) the SiC wafer was dried by nitrogen gas; (3) a photoresist (S1813) layer was coated on the surface of the SiC wafer and then exposed to ultraviolet light through a Cr mask; (4) a 400 nm thick Cu layer was deposited on the photoresist after development using e-beam evaporation (OHMIKER-50B); (5) a Cu mask with disc-shaped pattern was obtained by a lift-off process (Fig. S5f); (6) A periodic array of pillars was obtained by etching the SiC wafer for 21 min using an ICP (SENTECH PTSA ICP-RIE ETCHER SI 500) with gas mixture SF_6/ O_2 = 24:6 sccm, gas pressure = 0.3Pa, ICP power = 500 W, RF power = 150W and bias voltage = 220V; (7) the Cu mask with disc-shaped pattern was removed by immersing the sample into concentrated nitric acid, acetone, isopropyl alcohol and de-ionized water for 10 min in turn (Fig. S5g); (8) a 400nm-thick Cu sacrificial layer was deposited the surface of SiC wafer with pillars using e-beam evaporation (OHMIKER-50B) (Fig. S5 h) after the SiC wafer had been blown by N_2.; (9) the Cu sacrificial layer coated on the surface of the SiC wafer was etched for 50 min using an ICP (SENTECH PTSA ICP-RIE ETCHER SI 500) with the same parameters as (6); (10) the CPDSS was finally obtained by immersing the SiC wafer into the concentrated nitric acid and de-ionized water for 1 min in turn.

Characterization: Morphology of the sample was characterized with scanning electron microscopy (SEM, Hitachi S4800). Hemispherical measurement of the absorptivity was performed with an integrating sphere (EQUINOX 55) under the normal incidence of light.

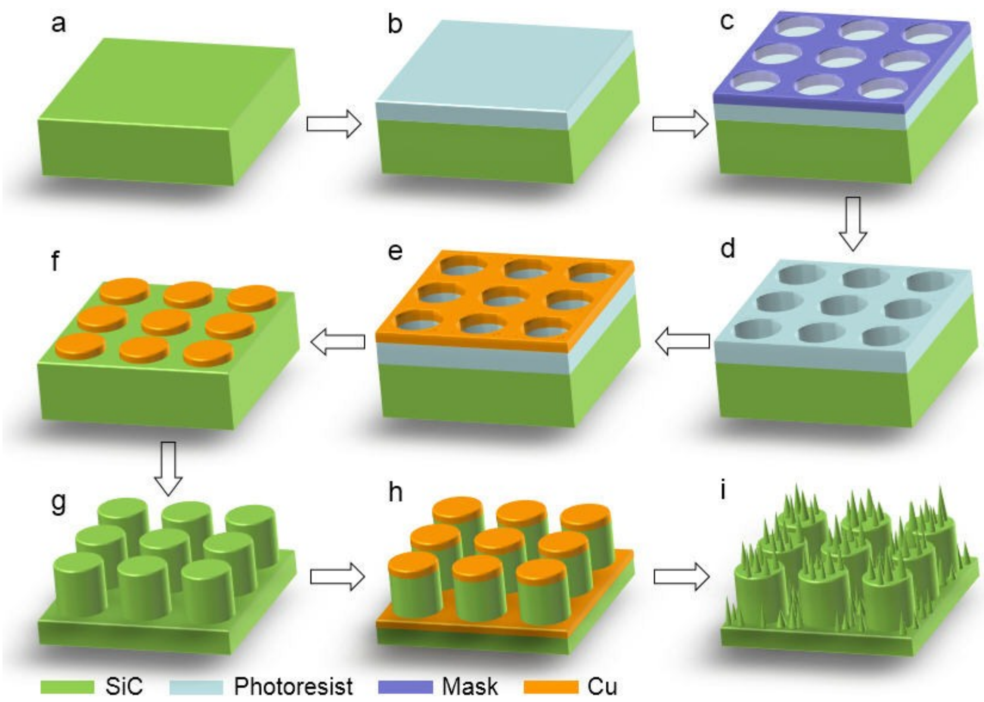

Figure S5. Fabrication procedure of the CPDSS. a) Single crystal 6H-SiC (0001) substrate. b) Ultraviolet photoresist coated on the substrate. c-d**)** Ultra-violet lithography and development. e-f) The fabrication of the Cu mask with disc-shaped patterns. g) ICP etching. h) A 400 nm thick Cu layer deposited using e-beam evaporation. i) The obtained CPDSS.

The pillar diameter D and the pillar period ($D+G$) of the SiC pillar array can be controlled by designing the pillar diameter and the pillar period of the Cu mask. The pillar height H of the SiC pillar array can be controlled by changing the thickness of the Cu mask and etching time. For example, a SiC pillar array with a pillar diameter of about $6\ \mu m$, a pillar period of $8\ \mu m$ and a pillar height of obout $8\ \mu m$ can be fabricated under the conditions that the pillar diameter and the pillar period of the Cu mask are $6\ \mu m$ and $8\ \mu m$, respectively, the thickness of the Cu mask is 100 nm and etching time is 10 min (see **Figure S10b**).

The cone height L, the cone diameter W and the cone density can be approximately controlled by changing thickness of Cu sacrificial layer (see **Figure S6**), etching time (see **Figure S7**) and etching power (see **Figure S8**). For example, a surface with only cones whose L is mainly located in the range from 4 μm to 5.7 μm, W is mainly located in the range from 0.4 μm to 0.7 μm and density is about 3.18/μm^2 can be fabricated under the conditions that the thickness of Cu sacrificial layer is 400 nm, etching time is 10 min and etching power is 150 W (see **Figure S10a**).

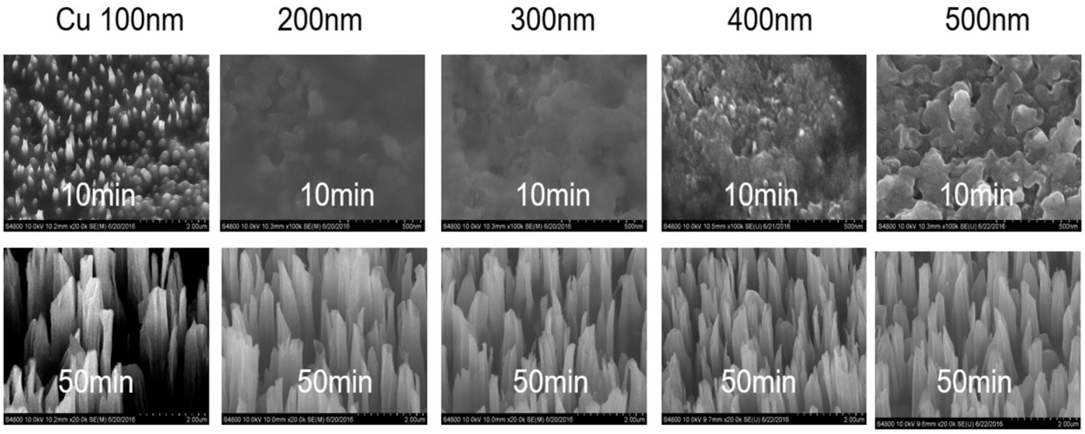

Figure S6. Variation of surface morphology of SiC with different thicknesses of Cu layer under an etching power of 150w. Thickness of sacrificial Cu layer is 100 nm, 200 nm, 300 nm, 400 nm, 500 nm, respectively, for etching time of 10 min and 50 min.

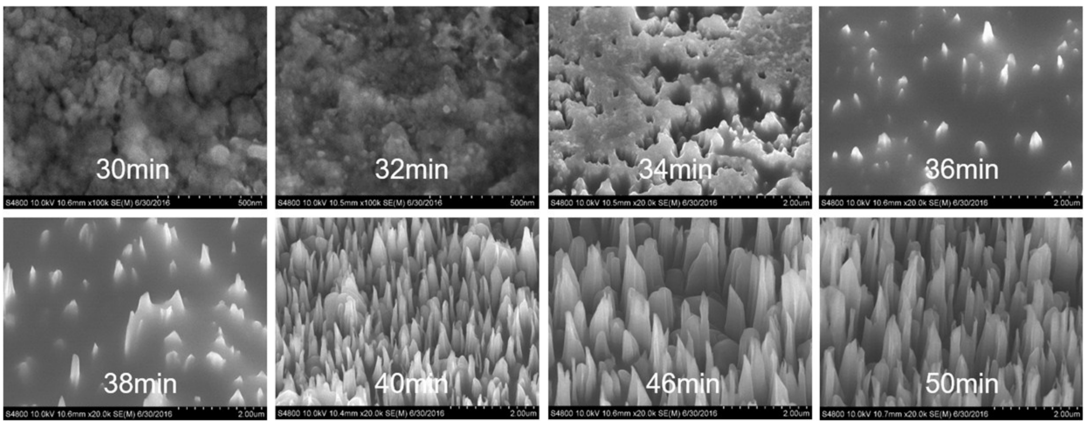

Figure S7. Variation of surface morphology of SiC with different etching times. The thickness of Cu sacrificial layer is 400nm, and etching power is 150w. Etching time is 30 min, 32 min, 34 min, 36 min, 38 min, 40 min, 46 min and 50 min, respectively.

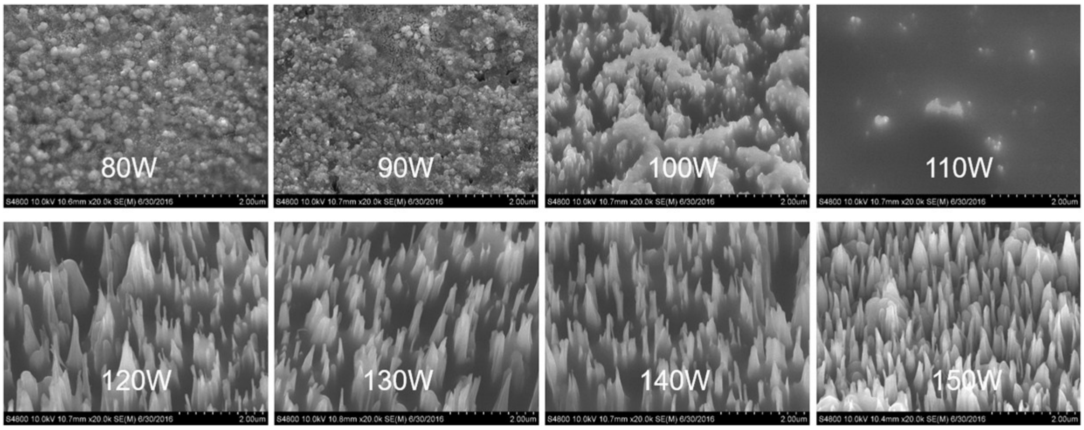

Figure S8. Variation of surface morphology of SiC with different etching powers. The thickness of Cu sacrificial layer is 400nm, and etching time is 40min. Etching power is 80 W, 90 W, 100 W, 110 W, 120 W, 130 W, 140 W and 150 W, respectively.

6. Comparison between the experimental result and the simulation result of the absorptivity

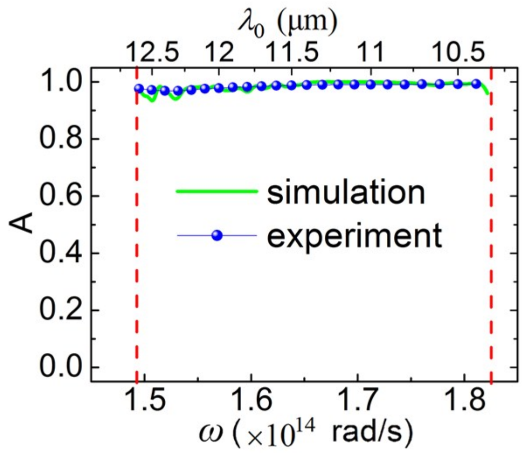

Figure S9. Comparison between the experimental result and the simulation result of the absorptivity. In this simulation, some grooves and ridges whose sizes are similar to that of grooves and ridges on the external sidewalls of the fabricated pillars are added to the sidewalls of the designed pillars. The curve of simulated A almost completely coincides with the curve of measured A in the whole RB.

7. SEM images of SiC simples

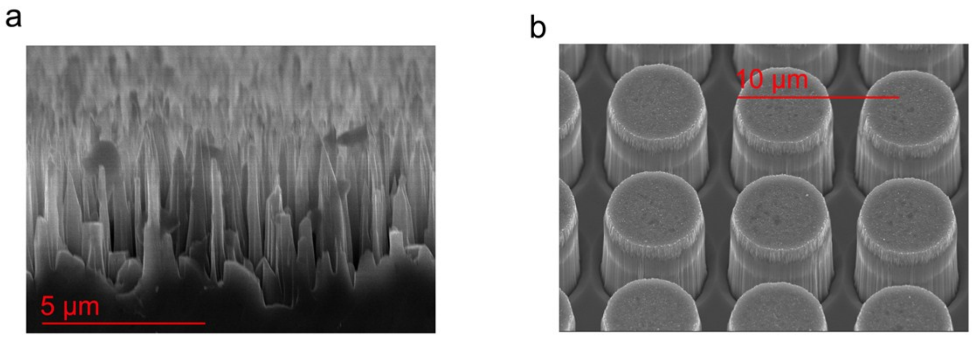

Figure S10. SEM images of SiC simples. a) A surface with only cones. b) A surface with only pillars.

8. Simulation results of the reflectivity and the absorptivity as a function of the incident angle

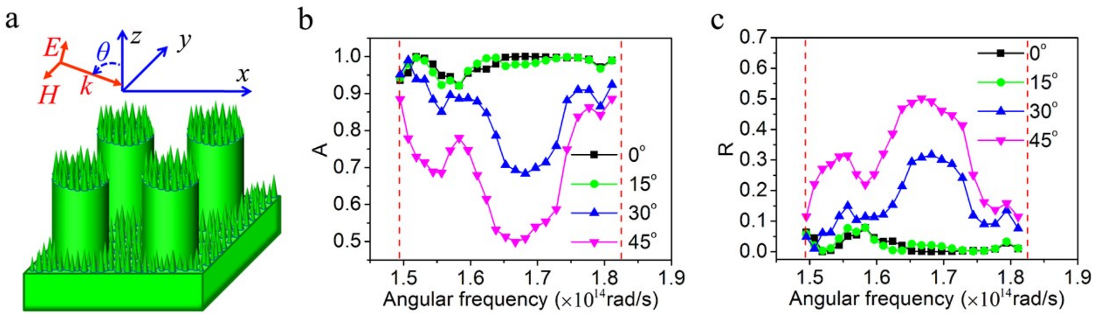

Figure S11. The reflectivity and the absorptivity vs. the incident angle. a) Incident angle θ of the incident linearly-polarized electromagnetic wave. b) The absorptivity A of a SiC with the CPDSS at incident angles of 0^{o}, 15^{o}, 30^{o} and 45^{o}. c) The reflectivity R of a SiC with the CPDSS at incident angles of 0^{o}, 15^{o}, 30^{o} and 45^{o}. The region between two red dashed lines is the RB.